Anomalous Nonlocal Conductance as a Fingerprint of Chiral Majorana Edge States

Satoshi Ikegaya,[1] Yasuhiro Asano,[2,3] and Dirk Manske[1]
[1]Max-Planck-Institut für Festkörperforschung, Heisenbergstrasse 1, D-70569 Stuttgart, Germany
[2]Department of Applied Physics, Hokkaido University, Sapporo 060-8628, Japan
[3]Center of Topological Science and Technology, Hokkaido University, Sapporo 060-8628, Japan

(Received 22 January 2019; revised manuscript received 22 May 2019; published 15 November 2019)

A chiral p-wave superconductor is the primary example of topological systems hosting chiral Majorana edge states. Although candidate materials exist, the conclusive signature of chiral Majorana edge states has not yet been observed in experiments. Here, we propose a smoking-gun experiment to detect the chiral Majorana edge states on the basis of theoretical results for the nonlocal conductance in a device consisting of a chiral p-wave superconductor and two ferromagnetic leads. The chiral nature of Majorana edge states causes an anomalously long-range and chirality-sensitive nonlocal transport in these junctions. These two drastic features enable us to identify the moving direction of chiral Majorana edge states in the single experimental setup.

DOI: 10.1103/PhysRevLett.123.207002

Introduction and main idea.—Superconductors (SCs) with spin-triplet chiral p-wave pairing symmetry have attracted intensive attention for the past two decades because they exhibit topologically protected chiral Majorana edge states (CMESs) having great potential applications to topological quantum computations [1,2]. According to a range of experimental [3–7] and theoretical [8–10] evidence, the perovskite superconductor Sr_2RuO_4 is the most promising candidate for the spin-triplet chiral p-wave SCs. At present, finding a smoking-gun signature of CMESs in this compound is an ongoing and central subject in both the physics of topological condensed matter [11–13] and that of spin-triplet superconductivity [14–16].

There have been three standard directions for the detection of CMESs. The first direction is by measurements of internal magnetic fields due to the spontaneous edge current [17–20]. However, the scanning superconducting quantum interference device experiments for Sr_2RuO_4 did not detect the expected fields [21,22] because of either the screening currents in the bulk [17] or for other reasons [23–25]. The second direction is by use of phenomena analogous to the quantum Hall effect in a two-dimensional electron gas with applied magnetic fields [26,27]: the spin quantum Hall effect [28] and thermal quantum Hall effect [29]. However, these effects have not been observed yet because of difficulties in spin and thermal transport measurements. The third direction studies anomalies in local charge transport of superconducting junctions, such as a zero-bias conductance peak in tunneling spectroscopy [30] and a low-temperature anomaly in Josephson currents [31]. However, roughly speaking, these anomalies can be induced by any type of midgap Andreev bound states and are not unique to the CMESs. Therefore, unfortunately, the zero-bias conductance peak observed in a planar tunneling experiment for Sr_2RuO_4 [32] cannot be the conclusive evidence for the CMESs.

To resolve this stalemate, in the present Letter, we propose a novel experiment that provide a smoking-gun signature of CMESs through charge transport measurements. The central ingredient of our scheme is that we measure nonlocal charge transport in the presence of CMESs [33]. We will use a setup as shown in Fig. 1, where two ferromagnetic (FM) leads are attached to an edge of a chiral p-wave SC [34]. The nonlocal conductance in a similar device replacing the chiral p-wave SC by a conventional s-wave SC has been already studied [35,36]. In such a device, the nonlocal conductance is governed by two distinctive nonlocal transport processes yielding opposite contributions: an incident electron from one lead is scattered into another lead as an electron (elastic

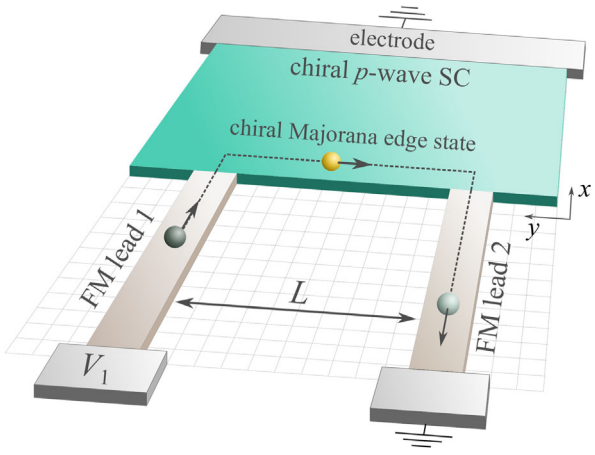

FIG. 1. Schematic image of the device consisting of a chiral p-wave superconductor with two ferromagnetic leads. Figure corresponds to the situation for measuring G_{21}.

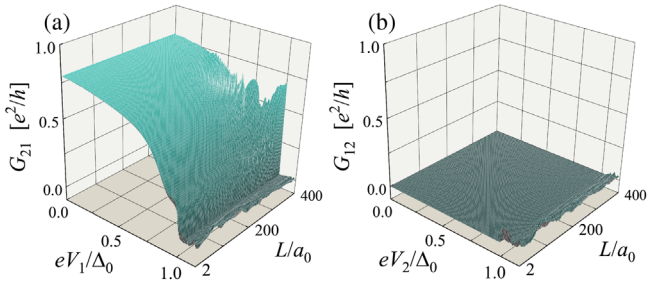

FIG. 2. Nonlocal conductance (a) G_{21} and (b) G_{12} are plotted as functions of the bias voltage and distance between the FM leads L. We vary L from $0.2\xi_0$ to $40\xi_0$. The spectrum of G_{21} and that of G_{12} are related to each other by changing the moving direction of the chiral Majorana edge states.

cotunneling process) or a hole (crossed Andreev reflection process). The exchange potential in the FM leads is a source of finite nonlocal conductance because it generates the imbalance between these two nonlocal transport processes [35,36]. With conventional s-wave SC, the subgap nonlocal conductance is strongly suppressed when the distance between the two leads exceeds the superconducting coherent length. This is because incident electrons must tunnel from one lead to the other through evanescent waves of Bogoliubov quasiparticles in the superconducting segment. However, we expect that CMESs modify the situation drastically such that the CMESs moving in the direction from lead α to β mediate the nonlocal transport from lead α to β insensible of the distance between the two leads, whereas they do not assist the nonlocal transport from lead β to α (see also Fig. 1). If we can capture such unusual anisotropy in the nonlocal transport processes, it can be a smoking-gun signature of the CMESs.

We calculate two types of nonlocal differential conductance, $G_{21} = dI_2/dV_1$ and $G_{12} = dI_1/dV_2$, by using the lattice Green function technique. Here, I_α is the current response in FM lead α due to the application of the bias voltage V_β to the electrode attached to FM lead β, where the electrodes attached to FM lead α and the superconductor are grounded. We will demonstrate that the spectra of G_{21} and G_{12} indeed exhibit the distinctive contrast reflecting the chiral motion of CMESs. Namely, when the CMESs move in the direction from lead α to β, the nonlocal conductance $G_{\beta\alpha}$ becomes finite even when the distance between the FM leads largely exceeds the superconducting coherent length, whereas the nonlocal conductance $G_{\alpha\beta}$ becomes almost zero (see Fig. 2). We can measure both G_{21} and G_{12} only by changing the lead wire to which the bias voltage is applied. Therefore, we can identify the moving direction of the CMES in the single experimental setup. The remarkable advantage of our proposal is that we only need the obvious difference in G_{21} and G_{12}, where one of them is finite and the other is zero, to identify the CMESs in the chiral p-wave superconductor conclusively.

Minimal model.—Let us consider the junction illustrated in Fig. 1 on a two-dimensional tight-binding model with lattice constant a_0. A lattice site is indicated by a vector $\boldsymbol{r} = j\boldsymbol{x} + m\boldsymbol{y}$, where $\boldsymbol{x}$ ($\boldsymbol{y}$) is the vector in the x (y) direction with $|\boldsymbol{x}| = |\boldsymbol{y}| = a_0$. The chiral p-wave SC occupies $j \geq 1$ and $-M_s \leq m \leq M_s$, where its width is given by $W_s/a_0 = 2M_s$. In the y direction, we apply the hard-wall boundary condition. FM lead 1 (FM lead 2) is placed on $j \leq 0$ and $m_f \leq m \leq M_f$ ($-m_f \geq m \geq -M_f$), where its width is denoted by $W_f/a_0 = M_f - m_f$. The distance between the two FM leads is given by $L/a_0 = 2m_f$. The present device is described by the Bogoliubov–de Gennes Hamiltonian $H = H_s + H_1 + H_2$. In this Letter, we phenomenologically describe the chiral p-wave SC by using the standard minimal model

$$H_s = \frac{1}{2}\sum_{\boldsymbol{r},\boldsymbol{r}'} \boldsymbol{c}_{\boldsymbol{r}}^\dagger \begin{bmatrix} \hat{\xi}^s_{\boldsymbol{r},\boldsymbol{r}'} & \hat{\Delta}_{\boldsymbol{r},\boldsymbol{r}'} \\ -\hat{\Delta}^*_{\boldsymbol{r},\boldsymbol{r}'} & -\hat{\xi}^s_{\boldsymbol{r},\boldsymbol{r}'} \end{bmatrix} \boldsymbol{c}_{\boldsymbol{r}'}, \tag{1}$$

where $j, j' > 0$,

$$\hat{\xi}^s_{\mathbf{r},\mathbf{r}'} = [-t_s\delta_{|\mathbf{r}-\mathbf{r}'|,a_0} + (4t_s - \mu_s)\delta_{\mathbf{r},\mathbf{r}'}]\hat{\sigma}_0,$$
$$\hat{\Delta}_{\mathbf{r},\mathbf{r}'} = \frac{\Delta_0}{2}[i(\delta_{j,j'+1} - \delta_{j+1,j'}) - \chi(\delta_{m,m'+1} - \delta_{m+1,m'})]\hat{\sigma}_x,$$

and $\boldsymbol{c}_{\boldsymbol{r}} = [c_{\boldsymbol{r},\uparrow}, c_{\boldsymbol{r},\downarrow}, c^\dagger_{\boldsymbol{r},\uparrow}, c^\dagger_{\boldsymbol{r},\downarrow}]^T$, with $c^\dagger_{\boldsymbol{r},\sigma}$ ($c_{\boldsymbol{r},\sigma}$) representing the creation (annihilation) operator of an electron at site $\boldsymbol{r}$ with spin σ ($= \uparrow$ or $\downarrow$). The Pauli matrices in spin space are represented by $\hat{\sigma}_i$ for $i = x$, y, and z; and the 2×2 unit matrix is denoted with $\hat{\sigma}_0$. t_s and μ_s, respectively, denote the nearest-neighbor hopping integral and the chemical potential in the superconductor. The amplitude and chirality of the pair potential are represented by Δ_0 and χ ($= 1$ or -1), respectively. The pair potential for a spin-triplet pairing symmetry in momentum space is generally described as $\hat{\Delta}(\boldsymbol{k}) = \boldsymbol{d}(\boldsymbol{k}) \cdot \hat{\boldsymbol{\sigma}}(i\sigma_y)$. In this Letter, we use the d vector of $\boldsymbol{d}(\boldsymbol{k}) = \Delta_0\hat{z}[\sin(k_x a_0) + i\chi \sin(k_y a_0)]$, which is the most probable one in Sr_2RuO_4 [8,9,14–16]. Here, k_x (k_y) represents the wave number along the x (y) direction, and $\hat{z}$ represents the unit vector in the z direction corresponding to the c axis of Sr_2RuO_4. FM lead α ($= 1, 2$) is described by

$$H_\alpha = \frac{1}{2}\sum_{\boldsymbol{r},\boldsymbol{r}'} \boldsymbol{c}_{\boldsymbol{r}}^\dagger \begin{bmatrix} \hat{\xi}^\alpha_{\boldsymbol{r},\boldsymbol{r}'} & 0 \\ 0 & -\hat{\xi}^\alpha_{\boldsymbol{r},\boldsymbol{r}'} \end{bmatrix} \boldsymbol{c}_{\boldsymbol{r}'}, \tag{2}$$

where $j \leq 0$,

$$\hat{\xi}^\alpha_{\boldsymbol{r},\boldsymbol{r}'} = [-t_f\delta_{|\boldsymbol{r}-\boldsymbol{r}'|,a_0} + (4t_f - \mu_f)\delta_{\boldsymbol{r},\boldsymbol{r}'}]\hat{\sigma}_0 + \boldsymbol{M}_\alpha \cdot \hat{\boldsymbol{\sigma}}\delta_{\boldsymbol{r},\boldsymbol{r}'}.$$

The nearest-neighbor hopping integral and the chemical potential in the FM leads are, respectively, denoted t_f

and μ_f. The exchange potential in FM lead α is given by $\boldsymbol{M}_\alpha = M_\alpha(\cos\theta_\alpha \sin\varphi_\alpha, \sin\theta_\alpha \sin\varphi_\alpha, \cos\varphi_\alpha)$. In what follows, we fix several parameters as $\mu_f = 1.0t_f$, $t_s = 1.0t_f$, $\mu_s = 2.0t_f$, $\Delta = 0.1t_f$, and $\chi = -1$. In the tight-binding model, the superconducting coherent length is given by $\xi_0 = (t_s/\Delta_0)a_0$ [37]. With our parameter choice, we obtain $\xi_0 = 10a_0$. The chiral p-wave SC hosts two CMESs originated from the two different spin sectors. With $\chi = -1$, both of them move along the edge at $j = 1$ in the direction from FM lead 1 to 2.

We are interested in the nonlocal differential conductances $G_{21}(eV_1) = dI_2/dV_1$ and $G_{12}(eV_2) = dI_1/dV_2$. On the basis of the Blonder-Tinkham-Klapwijk (BTK) formalism [38], the nonlocal conductance at zero temperature is given by [35,36,39–44]

$$G_{\beta\alpha}(eV_\alpha) = \frac{e^2}{h}[-R^{\mathrm{EC}}_{\beta\alpha} + R^{\mathrm{CAR}}_{\beta\alpha}]_{eV_\alpha = E}, \tag{3}$$

$$R^{\mathrm{EC(CAR)}}_{\beta\alpha} = \sum_{\zeta,\eta} |r^{ee(\mathrm{he})}_{\beta\alpha}(\zeta;\eta)|^2, \tag{4}$$

with $\alpha \neq \beta$. The elastic cotunneling (EC) and crossed Andreev reflection (CAR) coefficients at energy E are, respectively, denoted by $r^{ee}_{\alpha\beta}(\zeta;\eta)$ and $r^{he}_{\alpha\beta}(\zeta;\eta)$, where the index ζ (η) labels the outgoing (incoming) channel in FM lead β (FM lead α). These reflection coefficients are obtained by using the lattice Green function technique [45,46] (see Supplemental Material [47] for the detailed calculation). In the BTK formalism, we assume that all currents following towards $x = +\infty$ ($x = -\infty$) in the superconductor (FM lead β) are absorbed into the ideal electrode, which is not described in the Hamiltonian explicitly. We note that the BTK formalism is quantitatively justified for bias voltages well below the superconducting gap.

Results on nonlocal conductance.—We first focus on the nonlocal conductance G_{21}. In Fig. 2(a), we show G_{21} as a function of the bias voltage and distance between the FM leads L. We choose the parameters as $W_f = 20a_0$ and $W_s = 500a_0$. We vary L from $0.2\xi_0$ to $40\xi_0$, where $\xi_0 = 10a_0$. For the FM leads, we consider the antiparallel magnetization along the z axis, where $\boldsymbol{M}_{1(2)} = +(-)M_{\mathrm{ex}}\hat{z}$ with $M_{\mathrm{ex}} = 0.5t_f$. We find that G_{21} for $eV \ll \Delta_0$ is almost independent of L and is finite for $L \gg \xi_0$. Specifically, at zero-bias voltage, we find $G_{21} \approx 0.79(e^2/h)$, irrespective of L. The anomalously long-range nonlocal transport in the present junction suggests that wave functions in the two different FM leads are mediated not by evanescent waves but by the propagating waves of CMESs. We will later confirm this statement by analyzing the wave functions in the present junction. Next, we discuss the nonlocal conductance G_{12}. In Fig. 2(b), we show G_{12} as a function of the bias voltage and L, where the parameters are chosen as same as those in Fig. 2(a). In contrast to G_{21}, we find that G_{12} with $eV < \Delta_0$ is almost zero for all L. This suggests that the CMESs moving in the direction from leads 1 to 2 cannot assist the nonlocal transport processes from leads 2 to 1. In the BTK formalism, we assume that the CMESs moving towards $x = +\infty$ are absorbed into the ideal electrode attached to the superconductor. To support this assumption, we also calculate the reflection and transmission probabilities at an ideal chiral p-wave SC/normal-metal interface, and we confirm that the incident CMESs are always scattered into the attached normal-metal (see Supplemental Material [47] for the detailed calculation). We confirm that G_{21} (G_{12}) for $eV < \Delta_0$ becomes zero (finite) by changing the sign of chirality from -1 to $+1$. Thus, the distinctive contrast between G_{21} and G_{12} is indeed related with the moving direction of the CMESs. We can measure both G_{21} and G_{12} by changing the FM lead wire to which the bias voltage is applied. Therefore, by comparing G_{21} and G_{12}, we can test the sign of chirality, and therefore the moving direction of CMESs, in the single experimental setup.

We now discuss the exchange potential dependence of the nonlocal conductance. In Fig. 3(a), we show the nonlocal conductance G_{21} at zero-bias voltage as a function of the exchange potential amplitude. We here consider either parallel or antiparallel alignment of magnetization along the z axis with $\boldsymbol{M}_1 = |M_{\mathrm{ex}}|\hat{z}$ and $\boldsymbol{M}_2 = M_{\mathrm{ex}}\hat{z}$. With this representation, the parallel (antiparallel) alignments of the magnetization are described with $M_{\mathrm{ex}} > 0$ ($M_{\mathrm{ex}} < 0$). We choose the parameters as $W_f = 20a_0$, $W_s = 500a_0$, and $L = 300a_0$. For the antiparallel (parallel) magnetization, G_{21} becomes positive (negative) finite, which leads to the relation of $R^{\mathrm{EC}}_{21} < R^{\mathrm{CAR}}_{21}$ ($R^{\mathrm{EC}}_{21} > R^{\mathrm{CAR}}_{21}$). When the d vector in the superconductor is parallel or antiparallel to the magnetic moment in the FM leads, Andreev reflection occurs between electron and hole states with opposite spins, whereas normal reflection occurs between equal-spin electrons [48–50]. Therefore, the antiparallel magnetization in the FM leads suppresses the equal-spin scattering process of EC, whereas it does not damage the CAR process. On the other hand, the parallel magnetization in the FM leads does not damage the EC process, whereas it disturbs the spin flip in the CAR process. This roughly explains the relation of $R^{\mathrm{EC}}_{21} < R^{\mathrm{CAR}}_{21}$ ($R^{\mathrm{EC}}_{21} > R^{\mathrm{CAR}}_{21}$) with the antiparallel (parallel) magnetization. In the absence of the exchange potential ($M_{\mathrm{ex}} = 0$), the nonlocal conductance G_{21} becomes zero due to the complete cancellation between the contributions from the EC and CAR processes (i.e., $R^{\mathrm{EC}}_{21} = R^{\mathrm{CAR}}_{21}$). When $|M_{\mathrm{ex}}|$ exceeds μ_f, only the spin-$\downarrow$ states remain at the Fermi level in FM lead 1 and the only spin-$\uparrow$ (-$\downarrow$) states remain at the Fermi level in FM lead 2 with the antiparallel (parallel) alignment of magnetization. Within such a half-metallic limit ($|M_{\mathrm{ex}}| > \mu_f$), we obtain $G_{21} \approx +(-)e^2/h$ with the antiparallel (parallel) magnetization. In Fig. 3(b), we show G_{21} at zero-bias voltage for various directions of the magnetization. The exchange potentials in FM lead 1 and FM lead 2 are, respectively, chosen as

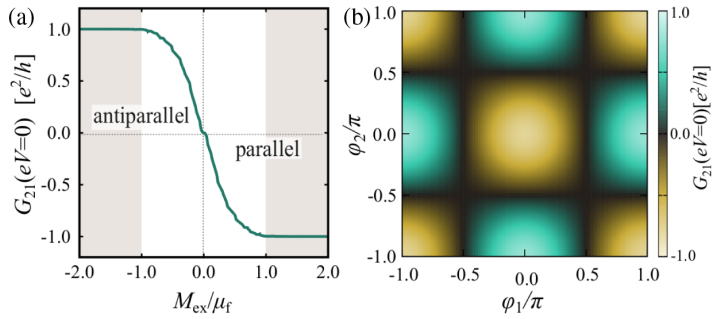

FIG. 3. (a) Nonlocal conductance G_{21} at zero-bias voltage as a function of the exchange potential $M_{\rm ex}$. (b) G_{21} at zero-bias voltage as a function of the angles of magnetic moments φ_1 and φ_2.

$\boldsymbol{M}_1 = M_{\rm ex}(\sin\varphi_1, 0, \cos\varphi_1)$ and $\boldsymbol{M}_2 = M_{\rm ex}(0, \sin\varphi_2, \cos\varphi_2)$ with $M_{\rm ex} = 0.5t_{\rm f}$. By changing φ_1 and φ_2, $\boldsymbol{M}_1$ and $\boldsymbol{M}_2$ are, respectively, rotated around the y and x axes. We choose the parameters as $W_{\rm f} = 20a_0$, $W_{\rm s} = 300a_0$, and $L = 160a_0$. Except for $\varphi_1 = \pm\pi/2$ and $\varphi_2 = \pm\pi/2$, we obtain the finite nonlocal conductance G_{21}. The sign of G_{21} is determined by $-{\rm sgn}(M_1^z){\rm sgn}(M_2^z)$, where $M_\alpha^z = M_{\rm ex}\cos\varphi_\alpha$. The maximum magnitude of G_{21} is obtained when both $\boldsymbol{M}_1$ and $\boldsymbol{M}_2$ are directed along either $+\hat{z}$ or $-\hat{z}$. We also confirm that the nonlocal conductance G_{12} is zero, irrespective of φ_1 and φ_2, for $L \gg \xi_0$. Therefore, we can find the distinctive contrast in G_{21} and G_{12} for the various alignments of the magnetization.

Majorana wave functions.—The anomalously long-range nonlocal transport in the present junction implies that an incident electron from one lead is transmitted through the superconducting segment as the CMESs, and it is scattered into other leads. To confirm this statement directly, we here analyze the quasiparticle wave functions contributing to the CAR process from FM leads 1 to 2. Specifically, we calculate the wave function

$$\psi_{\eta_{\rm M}}(\boldsymbol{r}) = [u_{\eta_{\rm M},\uparrow}(\boldsymbol{r}), u_{\eta_{\rm M},\downarrow}(\boldsymbol{r}), v_{\eta_{\rm M},\uparrow}(\boldsymbol{r}), v_{\eta_{\rm M},\downarrow}(\boldsymbol{r})]^{\rm T}$$

at zero energy, where η_M labels the incoming channel having the largest contribution to $R_{21}^{\rm CAR}$; i.e., η_M has the largest value of

$$\sum_{\zeta} |r_{21}^{he}(\zeta;\eta)|^2$$

among all η. Details for the calculation are given in the Supplemental Material [47]. To discuss the most comprehensible case, we assume the half-metallic ferromagnets with the antiparallel magnetization along the z axis, where $\boldsymbol{M}_{1(2)} = +(-)M_{\rm ex}\hat{z}$ with $M_{\rm ex} = 1.5\mu_{\rm f}$. With this specific choice of magnetization, $\psi_{\eta_M}(\boldsymbol{r})$ consists of only a spin-$\downarrow$ electron component $u_{\eta_M,\downarrow}$ and a spin-$\uparrow$ hole component $v_{\eta_M,\uparrow}$, whereas $u_{\eta_M,\uparrow} = v_{\eta_M,\downarrow} = 0$. Moreover, the local Andreev reflection in FM lead 1 and the EC from FM leads 1 to 2 are absent. In Figs. 4(a) and 4(b), we, respectively, show the spatial profile of the electron component amplitude $|u_{\eta_M,\downarrow}|$ and that of the hole component amplitude $|v_{\eta_M,\uparrow}|$. We choose the parameters as $W_f = 30a_0$, $W_s = 400a_0$, and $L = 200a_0$. In lead 1, we find the finite $|u_{\eta_M,\downarrow}|$, which corresponds to the incident electron wave and the normal-reflected electron wave. In lead 2, we find the finite $|v_{\eta_M,\uparrow}|$ corresponding to the crossed Andreev reflected hole wave. There are no propagating hole (electron) waves in lead 1 (lead 2) due to the absence of the local Andreev reflection (EC) process. For the superconducting segment, most importantly, we find that the wave function localized at the edge of the superconductor mediates the wave functions in the two different FM leads. To examine this in more detail, in Fig. 4(c), we show the ratio of $R = |u_{\eta_M,\downarrow}|/|v_{\eta_M,\uparrow}|$ at the edge of the superconductor ($j = 1$). We find that $R = 1.0$ holds between the two FM leads ($-100 < m < 100$). Therefore, the wave function bridging the two FM leads indeed corresponds to a Majorana edge excitation described by the superposition of an electron wave and a hole wave with equal amplitude.

Discussion.—In the present junction, we can obtain the nonlocal conductance as extremely insensitive to the distance between two FM leads because the propagating

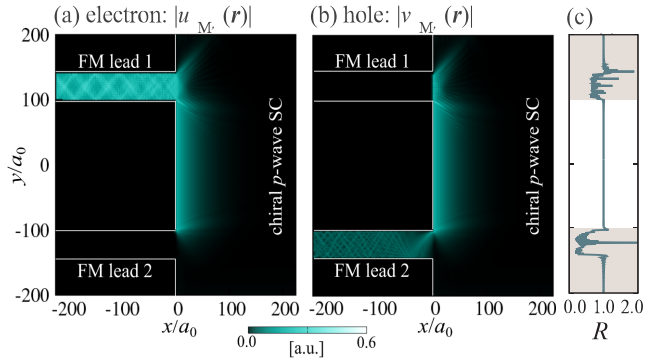

FIG. 4. Spatial profile of the wave function having the largest contribution to $R_{21}^{\rm CAR}$. In (a) and (b), we respectively show the amplitude of electron component $|u_{\eta_{\rm M},\downarrow}(\boldsymbol{r})|$ and that of hole component $|v_{\eta_{\rm M},\uparrow}(\boldsymbol{r})|$. In (c), the ratio of $R = |u_{\eta_{\rm M},\downarrow}|/|v_{\eta_{\rm M},\uparrow}|$ at the edge of the superconductor ($j = 1$) is plotted as a function of y.

CMESs mediating the nonlocal transport are irrelevant to the limitation from the superconducting coherent length. Here, we highlight the most significant advantage of our proposal: that we can identify the CMESs thorough the obvious difference in G_{21} and G_{12}, where one of them is finite and the other is zero. In real experiments, several perturbations (such as the tilt of the d vector and the spin-orbit coupling potentials in the vicinity of the junction interface) may induce additional spin-flip scattering processes and may decrease the amplitude of the finite nonlocal conductance. Even so, our proposal is still valid in the presence of such perturbations because we only need the contrast between the finite and the zero nonlocal conductances for detecting the CMESs. Actually, we have confirmed that the significant contrast between G_{21} and G_{12} is preserved for the broad range of magnetization alignments, as shown in Fig. 3(b). We also confirm that the substantial contrast in the conductance spectra is obtained, even in the presence of the next-nearest-neighbor pairing term in the pair potential [24,25] (see also the Supplemental Material [47]).

In summary, the nonlocal conductance in a device consisting of a chiral p-wave SC and two FM leads is studied within the mean-field theory. The CMESs cause the anomalously long-range and chirality-sensitive nonlocal transport and generate the drastic contrast in G_{21} and G_{12}. On the basis of these numerical results, we have proposed a smoking-gun experiment to detect the CMESs in chiral p-wave superconductors and have discussed the advantage of our proposal. We hope that our work will motivate further experiments on nonlocal transport measurements for recently fabricated ferromagnetic-$SrRuO_3$/Sr_2RuO_4 hybrid systems [51].

We are grateful to J. Annett, D. Schlom, J. Robinson, and S. Yonezawa for fruitful discussions. Y. A. is supported by "Topological Materials Science" (No. JP15H05852 and No. JP15K21717) from the Ministry of Education, Culture, Sports, Science and Technology of Japan; the JSPS Core-to-Core Program (A. Advanced Research Networks).

[1] N. Read and D. Green, Phys. Rev. B **61**, 10267 (2000).
[2] D. A. Ivanov, Phys. Rev. Lett. **86**, 268 (2001).
[3] Y. Maeno, H. Hashimoto, K. Yoshida, S. Nishizaki, T. Fujita, J. G. Bednorz, and F. Lichtenberg, Nature (London) **372**, 532 (1994).
[4] H. Murakawa, K. Ishida, K. Kitagawa, Z. Q. Mao, and Y. Maeno, Phys. Rev. Lett. **93**, 167004 (2004).
[5] G. M. Luke, Y. Fudamoto, K. M. Kojima, M. I. Larkin, J. Merrin, B. Nachumi, Y. J. Uemura, Y. Maeno, Z. Q. Mao, Y. Mori, H. Nakamura, and M. Sigrist, Nature (London) **394**, 558 (1998).
[6] K. Ishida, H. Mukuda, Y. Kitaoka, K. Asayama, Z. Q. Mao, Y. Mori, and Y. Maeno, Nature (London) **396**, 658 (1998).
[7] J. Xia, Y. Maeno, P. T. Beyersdorf, M. M. Fejer, and A. Kapitulnik, Phys. Rev. Lett. **97**, 167002 (2006).
[8] T. M. Rice and M. Sigrist, J. Phys. Condens. Matter **7**, L643 (1995).
[9] Y. Yanase and M. Ogata, J. Phys. Soc. Jpn. **72**, 673 (2003).
[10] Q. H. Wang, C. Platt, Y. Yang, C. Honerkamp, F. C. Zhang, W. Hanke, T. M. Rice, and R. Thomale, Europhys. Lett. **104**, 17013 (2013).
[11] M. Z. Hasan and C. L. Kane, Rev. Mod. Phys. **82**, 3045 (2010).
[12] X.-L. Qi and S.-C. Zhang, Rev. Mod. Phys. **83**, 1057 (2011).
[13] M. Sato and Y. Ando, Rep. Prog. Phys. **80**, 076501 (2017).
[14] A. P. Mackenzie and Y. Maeno, Rev. Mod. Phys. **75**, 657 (2003).
[15] Y. Maeno, S. Kittaka, T. Nomura, S. Yonezawa, and K. Ishida, J. Phys. Soc. Jpn. **81**, 011009 (2012).
[16] C. Kallin, Rep. Prog. Phys. **75**, 042501 (2012).
[17] M. Matsumoto and M. Sigrist, J. Phys. Soc. Jpn. **68**, 994 (1999).
[18] A. Furusaki, M. Matsumoto, and M. Sigrist, Phys. Rev. B **64**, 054514 (2001).
[19] M. Stone and R. Roy, Phys. Rev. B **69**, 184511 (2004).
[20] S.-I. Suzuki and Y. Asano, Phys. Rev. B **94**, 155302 (2016).
[21] P. G. Björnsson, Y. Maeno, M. E. Huber, and K. A. Moler, Phys. Rev. B **72**, 012504 (2005).
[22] J. R. Kirtley, C. Kallin, C. W. Hicks, E.-A. Kim, Y. Liu, K. A. Moler, Y. Maeno, and K. D. Nelson, Phys. Rev. B **76**, 014526 (2007).
[23] A. Bouhon and M. Sigrist, Phys. Rev. B **90**, 220511(R) (2014).
[24] W. Huang, S. Lederer, E. Taylor, and C. Kallin, Phys. Rev. B **91**, 094507 (2015).
[25] T. Scaffidi and S. H. Simon, Phys. Rev. Lett. **115**, 087003 (2015).
[26] K. V. Klitzing, G. Dorda, and M. Pepper, Phys. Rev. Lett. **45**, 494 (1980).
[27] D. J. Thouless, M. Kohmoto, M. P. Nightingale, and M. denNijs, Phys. Rev. Lett. **49**, 405 (1982).
[28] T. Senthil, J. B. Marston, and M. P. A. Fisher, Phys. Rev. B **60**, 4245 (1999).
[29] A. Vishwanath, Phys. Rev. Lett. **87**, 217004 (2001).
[30] M. Yamashiro, Y. Tanaka, and S. Kashiwaya, Phys. Rev. B **56**, 7847 (1997).
[31] Y. Asano and K. Katabuchi, J. Phys. Soc. Jpn. **71**, 1974 (2002).
[32] S. Kashiwaya, H. Kashiwaya, H. Kambara, T. Furuta, H. Yaguchi, Y. Tanaka, and Y. Maeno, Phys. Rev. Lett. **107**, 077003 (2011).
[33] I. Serban, B. Béri, A. R. Akhmerov, and C. W. J. Beenakker, Phys. Rev. Lett. **104**, 147001 (2010).
[34] S. B. Chung, S. K. Kim, K. H. Lee, and Y. Tserkovnyak, Phys. Rev. Lett. **121**, 167001 (2018).
[35] G. Deutscher and D. Feinberg, Appl. Phys. Lett. **76**, 487 (2000).
[36] T. Yamashita, S. Takahashi, and S. Maekawa, Phys. Rev. B **68**, 174504 (2003).
[37] A. C. Potter and P. A. Lee, Phys. Rev. Lett. **105**, 227003 (2010).
[38] G. E. Blonder, M. Tinkham, and T. M. Klapwijk, Phys. Rev. B **25**, 4515 (1982).
[39] C. Benjamin and J. K. Pachos, Phys. Rev. B **78**, 235403 (2008).

[40] F. Crépin, P. Burset, and B. Trauzettel, Phys. Rev. B **92**, 100507(R) (2015).
[41] A. Soori and S. Mukerjee, Phys. Rev. B **95**, 104517 (2017).
[42] R. Beiranvand, H. Hamzehpour, and M. Alidoust, Phys. Rev. B **96**, 161403(R) (2017).
[43] T. Ö. Rosdahl, A. Vuik, M. Kjaergaard, and A. R. Akhmerov, Phys. Rev. B **97**, 045421 (2018).
[44] K. Zhang and Q. Cheng, Supercond. Sci. Technol. **31**, 075001 (2018).
[45] P. A. Lee and D. S. Fisher, Phys. Rev. Lett. **47**, 882 (1981).
[46] T. Ando, Phys. Rev. B **44**, 8017 (1991).
[47] See Supplemental Material at http://link.aps.org/supplemental/10.1103/PhysRevLett.123.207002 for the detailed calculations for the nonlocal conductance and the wave function in the present junction. We also discuss the transmission probability of chiral p-wave superconductor/normal-metal interface, and the nonlocal conductance in the presence of the next-nearest neighbor pairing.
[48] N. Yoshida, Y. Tanaka, J. Inoue, and S. Kashiwaya, J. Phys. Soc. Jpn. **68**, 1071 (1999).
[49] T. Hirai, N. Yoshida, Y. Tanaka, J.-I. Inoue, and S. Kashiwaya, J. Phys. Soc. Jpn. **70**, 1885 (2001).
[50] T. Hirai, Y. Tanaka, N. Yoshida, Y. Asano, J. Inoue, and S. Kashiwaya, Phys. Rev. B **67**, 174501 (2003).
[51] M. S. Anwar, S. R. Lee, R. Ishigro, Y. Sugimoto, Y. Tano, S. J. Kang, Y. J. Shin, S. Yonezawa, D. Manske, H. Takayanagi, T. W. Noh, and Y. Maeno, Nat. Commun. **7**, 13220 (2016).